Electronic Structure of a Neodymium(III) tris(oxydiacetate) Complex from Luminescence data and *ab initio* Calculations

*Villads R. M. Nielsen[†‡], Maxime Grasser[‡], Sabina Svava Mortensen[†], Boris Le Guennic[‡], and Thomas Just Sørensen[†]**

[†] Department of Chemistry & Nano-Science Centre, University of Copenhagen, Universitetsparken 5, 2100 Copenhagen, Denmark, tjs@chem.ku.dk

[‡] Univ Rennes, CNRS, ISCR (Institut des Sciences Chimiques de Rennes), UMR 6226, F-35000 Rennes, France

Abstract

Neodymium(III) is a NIR emissive and magnetic ion, which has found use in various high-technology applications. Yet, accurate predictions of the luminescent and magnetic properties of neodymium(III) based on the coordination environment remain to be done. Guideline exists, but to build structure-property relationships for this element, more data are needed. Herein, we present a high-symmetry starting point. The tris(oxydiacetate) complex of neodymium(III) was prepared and crystallised, and access to the experimentally determined structure allows us to quantify the symmetry of the compound and to perform calculations directly on the same structure that is

investigated experimentally. The luminescent properties were determined and the electronic structure was computed using state-of-the-art *ab initio* methods. All electronic transitions in the range from 490 to 1400 nm were mapped experimentally. Using a Boltzmann population analysis, the combination of the excitation and emission spectra revealed the crystal field splitting of the 18 lowest energy Kramers levels that experimentally could be unambiguously resolved. This assignment was supported by *ab initio* calculations and the crystal field splitting was well reproduced. The electronic structure reported for the tris(oxydiacetate) complex is used to deduce the coordination structure in aqueous solution. Finally, the results are compared to empirical trends in the literature for the electronic structure of neodymium(III).

TOC

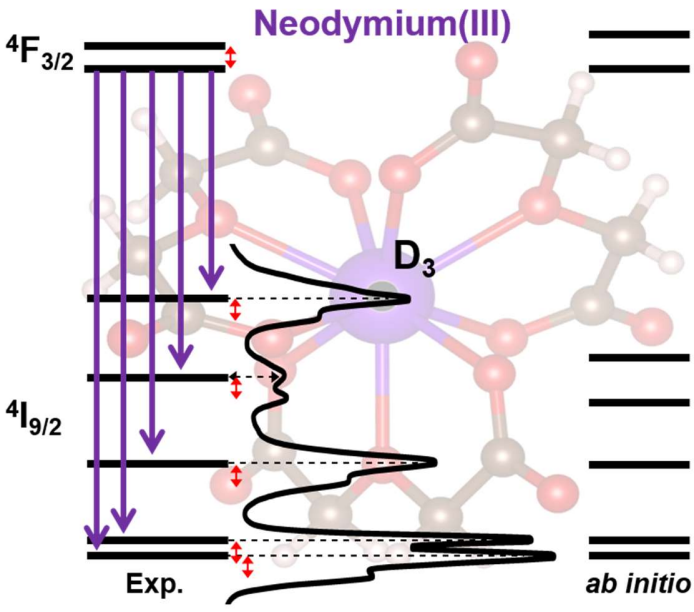

Introduction

Neodymium is today the primary active element used in modern high-power lasers,[1-3] and permanent magnets.[4, 5] These applications exploit the unique and fascinating luminescent and magnetic properties found in all lanthanides, but the case of neodymium has proven to revolutionize these industries.[1-5] Luminescence and magnetism of the lanthanide ions are inherently linked, and both arise from the electronic structure dictated by the *f*-electrons.[6] Thus, revealing the effects of the coordination environment on the electronic structure is a step further into the control and predictability of these societal impactful properties.

Throughout the periodic table, lanthanide-based luminescence is unique. The visible and NIR transitions are atom-like resulting in recognizable narrow bands in both absorption and emission. The emissive states are long lived, which can be exploited in bioimaging and biological probes,[7-9] up-conversion materials,[10, 11] and ratiometric luminescent thermometry.[12-15] The NIR imaging lanthanide ions, such as neodymium(III), ytterbium(III), and erbium(III) are of particular interest,[15-19] since biological tissue is transparent in their optical active range.[20-22] Neodymium(III) has four emission bands: $^4F_{3/2} \rightarrow {}^4I_{9/2}$, $^4F_{3/2} \rightarrow {}^4I_{11/2}$, $^4F_{3/2} \rightarrow {}^4I_{13/2}$, and $^4F_{3/2} \rightarrow {}^4I_{15/2}$ extending from 850 nm to 1700 nm, and can be excited in wide optical window ranging from deep into the UV into the NIR. From the VIS to NIR the bands $^4I_{9/2} \rightarrow {}^4F_{3/2}$, $^4I_{9/2} \rightarrow {}^4F_{5/2}$, $^4I_{9/2} \rightarrow {}^2H_{9/2}$, $^4I_{9/2} \rightarrow {}^4F_{7/2}$, $^4I_{9/2} \rightarrow {}^2S_{7/2}$, $^4I_{9/2} \rightarrow {}^4F_{9/2}$, $^4I_{9/2} \rightarrow {}^2H_{11/2}$, $^4I_{9/2} \rightarrow {}^4G_{5/2}$, $^4I_{9/2} \rightarrow {}^4G_{7/2}$, $^4I_{9/2} \rightarrow {}^2K_{13/2}$, and $^4I_{9/2} \rightarrow {}^4G_{9/2}$ can be excited from 500 nm to 900 nm and have a wide potential for probing biological tissues.[23]

Furthermore, the narrow absorption and emission lines of the lanthanides(III) contain valuable information on electronic structure that allows us to use optical spectroscopy as a tool to study the molecular structure of neodymium(III) containing compounds.[23-26] In this work, the electronic

structure is unambiguously extracted in solution by careful analysis,[27] and the nature and energy of each of the 20 electronic states in the $^4I_{9/2}$, $^4I_{11/2}$, $^4I_{13/2}$, and $^4F_{3/2}$ multiplets of the neodymium(III) ion are resolved in combination with *ab initio* calculations.[28] Since the 4*f* subshell of neodymium(III) is filled with an odd number of electrons, all electronic states are doubly degenerate and are described as Kramers doublets.[23] *Ab initio* multiconfigurational calculations as CASSCF (complete active space self-consistent field) including spin-orbit (SO) coupling have already proven to be a reliable and robust approach to calculate the electronic structure of the ground state multiplets in lanthanide complexes.[29-35] For researches focusing on molecular magnetism, luminescence is often used to validate the electronic structure obtained from *ab initio* calculations used to model the magnetic measurements.[36, 37] This approach has been extensively used on dysprosium(III),[31, 32, 38-41] terbium(III),[42, 43] and ytterbium(III).[33-35, 44-47] These elements are commonly studied for their single molecule magnet behaviour. Neodymium(III) can also display such behaviour and *ab initio* calculations at the CASSCF level have been able to map the 5 lowest states in the $^4I_{9/2}$ multiplet, and thus reproduce the observed magnetic behaviour.[48-52] However, for neodymium(III), limited reports on the performance of *ab initio* calculated electronic structures compared to experimentally determined electronic structures can be found,[23] and—to our knowledge—no reports on how *ab initio* calculations reproduce higher energy multiplets in neodymium(III) has been published yet.

As a model system, we selected a luminescent neodymium(III) tris(oxydiacetate) complex $Nd(ODA)_3$, which crystallized as compound $Na_3[Nd(ODA)_3]\cdot 10H_2O$ in a crystallographic phase not previously reported. This family of $Ln(ODA)_3$ complexes has been shown to crystallise in an array of different phases,[53-56] and the structure of the complexes is often reported to adopt a tricapped trigonal prismatic (TTP) coordination geometry.[56] Previously reported $Ln(ODA)_3$

compounds crystallise with three Na^+ counter ions in the monoclinic *C*2/*c* and *Cc* space groups. These structures have been reported for Eu^{3+} and Gd^{3+} (CCDC entries DOFXIF 1143446, DOFIX01 209363, and QUMYON 721017).[55, 57, 58] However, the neodymium(III) compound was found to crystallise in the triclinic *P*-1 space group (CCDC entry 2303145). Previously, only the isostructural cerium(III) compound has been reported with this space group (CCDC entry ODACCE01).[59] $Ln(ODA)_3$ compounds have already proven their interests in terms of magnetic properties, circular polarised luminescence, and supramolecular assemblies,[60-63] and the $Ln(DPA)_3$ coordination backbone of similar structure as $Ln(ODA)_3$ is similarly attracting interest.[33, 64, 65] We have studied these C_3 symmetric coordination backbones as model systems for the electronic structure of some lanthanides based on luminescence.[66] A recent *ab initio* work on the electronic structure of lanthanide(III) ion calculated the crystal field splitting in an isostructural series of $Ln(ODA)_3$ but without any experimental validation, and excluding neodymium(III) from the series.[67] Here, we resolve the electronic structure of the 18 lowest-lying energy states and the 2 emitting states in $Nd(ODA)_3$ spectroscopically. We evaluate these results in light of *ab initio* calculations and find the calculations to be in good agreement with experimental results in terms of energy splitting for both the lower ^4I_J multiplets and the emitting states. Additionally, we deduce that the structure of $Nd(ODA)_3$ in solution is identical to the one in the crystal based on similarities in the luminescent spectra.[33, 64, 65, 68]

Experimental Section

Synthesis and Crystallisation

$Nd(CF_3SO_3)_3$ (1183 mg, 2.000 mmol) (98% from TCI) was used to create a 0.20 M stock solution by dissolving the salt in water creating a solution with a volume of 10.0 ± 0.06 ml. H_2ODA (536.3 mg, 4.00 mmol) (H_2ODA from Sigma-Aldrich), H_2ODA = 2,2'-oxodiacetate, was used to

create a 0.20 M stock solution by dissolving the acid in water to create a solution with a volume of 20 ± 0.04 ml with pH = 5 using NaOH (1.0 M). 0.5 ml of the 0.2 M $Nd(CF_3SO_3)_3$ was added to a sample vial with 1.5 ml of the 0.2 M H_2ODA stock. The sample was heated at 80°C for 1 h. At this point the solution spectra were measured. The sample vial was placed in a container with acetone. A lid was then placed on top and the sample was left for acetone diffusion. After 2 days crystals had formed. The crystals are shown in Figure S1.

Single Crystal X-ray Diffraction

Single-crystal X-ray diffraction data were collected on a Bruker D8 Venture diffractometer equipped with a PHOTON 100 CMOS detector, a multilayer X-ray mirror, and a Mo Kα high brilliance IμS X-ray tube (λ = 0.71073 Å). The temperature was kept at 100 K using an Oxford Cryo system.

The crystal structure was solved using Olex2[69] with the ShelXT program[70] using intrinsic phasing. The ShelXL[71] refinement package with least square minimisation was used for refinement of the structure. Non-hydrogen atoms were refined anisotropically. Hydrogen atoms from water molecules were located using residual density after having assigned the other atoms. The rest of the hydrogen atoms were added automatically using a riding model. The crystal data is provided in Table S1.

Powder X-ray Diffraction

The crystals were chorused into a powder and were dispersed on a low background silica sample holder ready for powder x-ray diffraction (PXRD). Powder X-ray diffraction was done on a Bruker D8 X-ray diffractometer with a Cu anode, providing an x-ray wavelength of λ = 1.5418Å). The PXRD was recorded at 293 K with an integration time of 1 s in the range 2θ = 5 to 50° with a

resolution of $\Delta 2\theta = 0.0277°$. XRD results show that the powder has the same phase as the single crystal seen in Figure S2.

Optical and NIR spectroscopy

Sample preparation. Single crystals were crushed into a powder and transferred to a 7" NMR tube from Bruker where 2-methyltetrahydrofuran was added to disperse the powder ready for measurements. Measurements done on powder were performed in these tubes both at room temperature (RT) and at 77 K, exposed to air and liquid nitrogen, respectively. Solution samples were created similarly to the synthesis of the crystals, but were not put into a bath of acetone. The prepared solution samples had 20 mM neodymium(III) and 60 mM H_2ODA in a volume of 5 mL. The pH was adjusted to 5 using NaOH.

Solution samples were measured within 2 hours of creation. RT measurements on solution samples have been done in 10 mm quartz cuvettes (23/Q/10) from Starna Scientific. Finally, solution samples were measured at 77K in the NMR tubes snap-frozen in liquid nitrogen. We detected no signals from other lanthanides in any spectra.

Emission spectra. All measurements were performed on a recently reported spectrometer.[72] The samples were excited by a supercontinuum laser (NKT SuperK Fianium FIU-15) that was coupled to a tunable band pass filter (NKT LLTF Contrast VIS/SWIR HP8). The laser power was set to 100% with maximum repetition rate (78MHz). A 750B grating and a PyLoN detector were used for measurements below the 950 nm point, and a 1200B grating and the NIRvana detector were used for measurements above 950 nm. The emission slit was set to 10 µm for all emission measurements. The 880 nm band was exposed for 2 seconds and the 1060 and 1350 nm bands were exposed for 60 seconds. The excitation wavelength was set to 580 nm (with a broadness of 2 nm), and a long pass filter of 750 nm was used on the emission side. A background has been

created for each measurement with identical acquisition and has been used for background subtraction. In the entire range we have a spectral resolution of 0.4 nm on the emission side.

Excitation spectra. At each excitation wavelength, an emission spectrum of the 1060 nm band was recorded with a slit size of 200 µm and an exposure rate of 500 ms. The intensities of the excitation spectra are the integrated emission of the 1060 nm band (integrated from 1045 to 1070 nm) for each excitation wavelength. The resolution on the excitation side is 2 nm.

***Ab initio* calculations**

The evaluation of the electronic structure was carried out with the software OpenMOLCAS (version 22.10).[73, 74] State average (SA) complete active space (CAS), and restricted active space (RAS) self-consistent field (SCF) approaches were used.[75-78] Relativistic corrections at the scalar level have been taken into account by the use of the Douglas-Kroll-Hess Hamiltonian[79-81] and the all-electron atomic natural orbital relativistic contracted (ANO-RCC) basis-set from the Molcas library.[82, 83] The following contractions were used: [8s7p4d3f2g1h] for the Nd element, [3s2p1d] for the C and O elements, and [2s] for the H element. Spin-orbit (SO) coupling has been added within the restricted active space state interaction (RASSI) method[84] on the number of previously calculated roots with the use of the atomic mean field integral (AMFI) theory.[85] SA-CAS(3,7)SCF/RASSI-SO calculations were carried out including three electrons spread in the seven 4f orbitals of the neodymium(III) ion. All spin-free states were calculated, that is 35 quadruplets and 112 doublets for neodymium(III) ion. These calculations were extended by SA-RAS[3,0,2,0,7,5]SCF/RASSI-SO calculations including the five 5*d* orbitals of the neodymium(III) ion. The *ab initio* calculations were performed on the molecular structure of $Nd(ODA)_3$ as taken from the crystal structure where the position of the hydrogen atoms have been optimized, H-Opt $Nd(ODA)_3$. The optimizations were performed using density functional theory (DFT),[86] with the

GGA-PBE exchange-correlation functional.[87] Calculations have been performed with the ADF suite (version 2022.101)[88, 89] with basis sets at the TZP level for all atoms. The ZORA formalism with the MAPA potential was used to describe scalar relativistic effects as implemented in ADF.[90, 91]

The final choice of basis set and geometry included in the calculations specified above was decided based on multiple calculations performed. These are briefly discussed in the supporting information (See Figure S12 and Tables S15-17). Based on these it was decided to perform the SA-RAS[3,0,2,0,7,5]SCF/RASSI-SO level calculations on the H-Opt $Nd(ODA)_3$ which was then found to best reproduce the experimentally determined electronic structure. The results from this calculation are the only results presented in the main text.

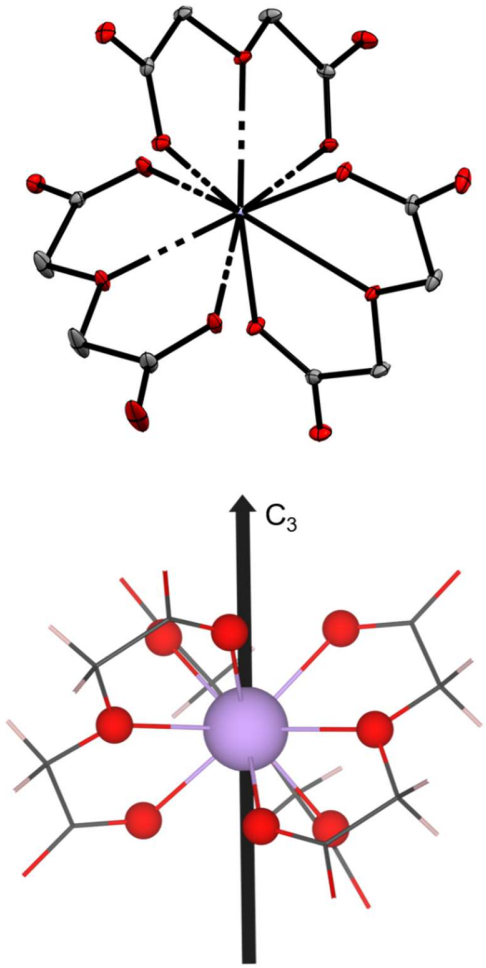

Figure 1. ORTEP figure (top) for the [Nd(ODA)$_3$] structure. Thermal ellipsoids are at 50% probability. Hydrogen atoms were omitted for clarity. Color code: C = Grey, Nd = purple, and O = red. Molecular structure (bottom) of Nd(ODA)$_3$ visualized with the C_3 symmetry axis. The C_3 axis is the optimized principal axis of the D_3 point group evaluated on the complex.

Results and discussion

Molecular structure

The molecular Nd(ODA)$_3$ complex within the Na_3[Nd(ODA)$_3$]·10H_2O crystal (CCDC entry 2303145) is shown in Figure 1 and crystal data are provided in Table S1. The structure was analysed with two methodologies to evaluate the coordination geometry: A geometry analysis

based on geometry deviation values from ideal polyhedron,[92] and a point group symmetry analysis based on how well symmetry operations in a point group operate on the structure (Equations S1-S2 for details).[93] With a deviation value of σ_{Ideal}(Q,TTP) = 1.15, the first coordination sphere is found to adopt a slightly distorted tricapped trigonal prismatic (TTP) geometry (See Table S2 for other geometries). This is in agreement with previously reported $[Nd(ODA)_3]^{3-}$ compounds.[94-98] The point group of the first coordination sphere is found to be slightly distorted from D_3 with a deviation value of $\sigma_{Sym}(Q, D_3) = 0.29$. Including the entire complex with the three ODA^{2-} molecules this deviation value increases to $\sigma_{Sym}(Q', D_3) = 1.3$. Based on our current experience with this methodology,[66, 93] we conclude that the coordination geometry has D_3 symmetry both in the inner sphere and in the entire molecular structure. The results of the point group analysis are compiled in Table 1. Comparing these results to the symmetry of $Ln(ODA)_3$ molecular structures (Q'') by Connolly *et al.*[67] we find their structure to be of perfect D_3 symmetry, with $\sigma_{Sym}(Q'', D_3) = 0.00$ for all their eight complexes (See Tables S3 and S4).

Table 1. Point group symmetry deviation in the first coordination sphere and in the molecular structure of the $Nd(ODA)_3$ structure.

Q	G:	C_{4v}	C_4	D_{3h}	D_3	C_3	C_2	C_i
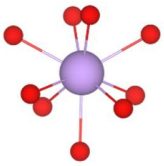	**First coordination-tion sphere**	3.3	3.5	1.9	**0.29**	0.35	0.11	41.1

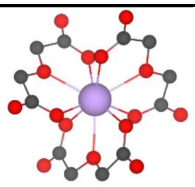	**$Nd(ODA)_3^{3-}$ molecular structure**	22.82	27.02	11.50	**1.30**	1.54	0.72	30.1

Spectroscopy data and experimental electronic structure

The trivalent neodymium(III) ion has an electronic configuration [Xe]$4f^3$. The three valence electrons can form 364 individual electronic states in 182 Kramers doublets.[23] Interelectronic repulsion and spin-orbit coupling split these into 41 multiplets classified with Russel-Saunders term symbols. The total energy splitting of these terms span 50,000 cm^{-1}. In Figure 2, the optical transitions between these multiplets are shown from 7,000 cm^{-1} to 20,000 cm^{-1} for the suspended $Na_3[Nd(ODA)_3]\cdot 10H_2O$ powder, determined from PXRD to have the same crystal phase as the single crystal in Figure S2 (See also Figures S3-5 and S7-10 for high-resolution spectra). Based on information from Carnall,[99] we are able to assign 14 bands in this range. $^4I_{9/2}$ is the lowest energy multiplet and all excitations at temperatures from 77 K to RT occur from the five Kramers doublets that constitute this multiplet. $^4F_{3/2}$ is the primary emitting multiplet and with a separation of ~1,000 cm^{-1} from the $^4F_{5/2}$ and $^2H_{9/2}$ manifold, it is assumed that all emission observed is from the two Kramers doublets in the $^4F_{3/2}$ multiplet.

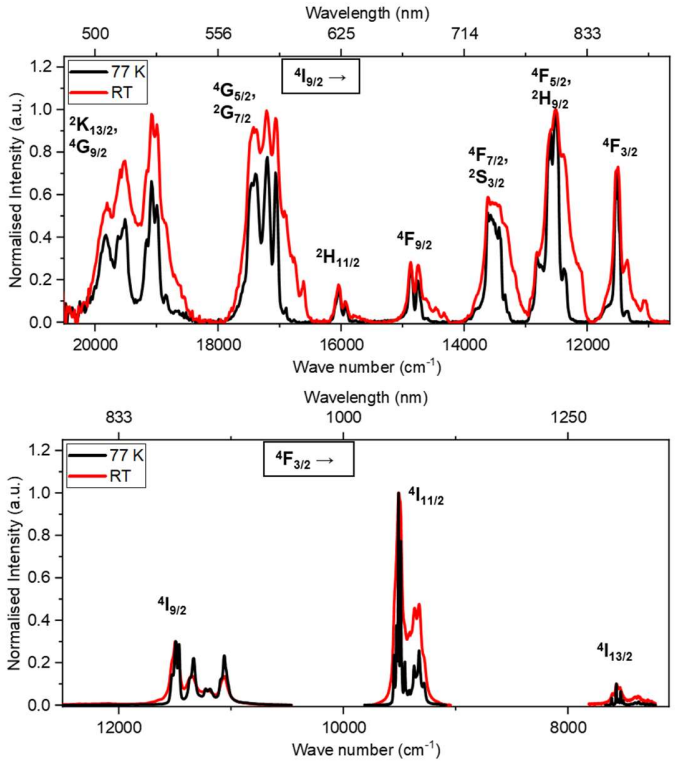

Figure 2. Excitation following 1045 to 1070 nm emission (top) and emission following 580 ± 1 nm excitation (bottom) spectra of the $Na_3[Nd(ODA)_3]\cdot 10H_2O$ crystal at 77 K and room temperature (RT) dispersed in 2-methyltetrahydrofuran.

On closer inspection of Figure 2, it can be seen that the change in temperature has a large impact on the excitation. At room temperature, each multiplet has a tail at the low energy side, which is not apparent in the low temperature data. This is rationalised from the depopulation of thermally populated states in $^4I_{9/2}$ upon cooling. A similar trend is not found for the emission data. Overall, all bands are broadened at room temperature compared to 77 K. Based on these observations and scrutiny of the transitions between $^4I_{9/2}$ and $^4F_{3/2}$ (see Figure S6), we conclude that these temperature dependencies can be described by a model where $^4I_{9/2}$ is split by approximately 400 cm^{-1} and $^4F_{3/2}$ is split by less than 50 cm^{-1}.

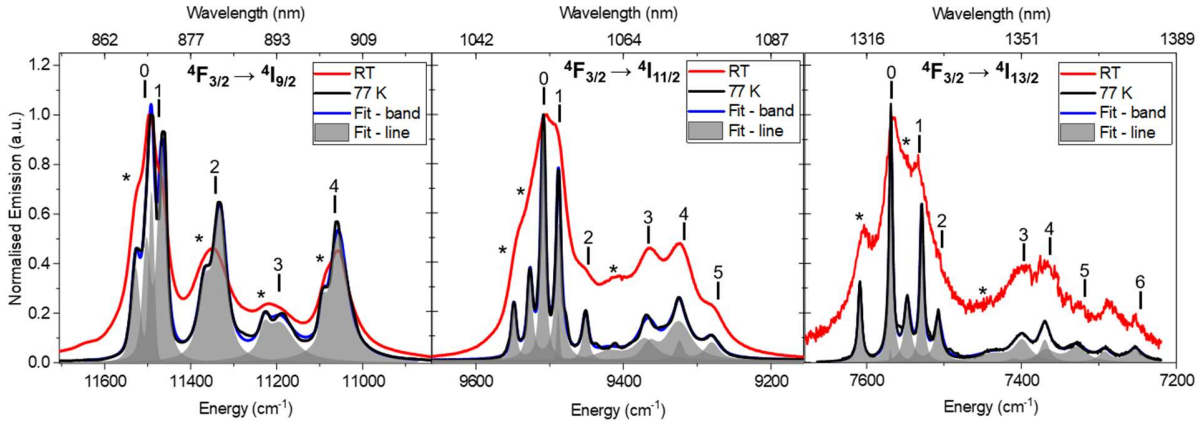

Figure 3. Emission of $^4F_{3/2} \rightarrow {}^4I_{9/2}$ (left), $^4F_{3/2} \rightarrow {}^4I_{11/2}$ (middle), and $^4F_{3/2} \rightarrow {}^4I_{13/2}$ (right) at 77 K and RT. Each band at 77 K has been fitted with Voigt functions shown in the figure. The final m_J-states in $^4F_{3/2}(0) \rightarrow {}^4I_J$ are highlighted as numbers starting from 0 to the number of possible lines equal to J – 1/2 and transitions easily recognized to originate from $^4F_{3/2}(1) \rightarrow {}^4I_J$ are highlighted with an asterisk.

Figure 3 shows three of the four luminescence bands observed for neodymium(III): $^4F_{3/2} \rightarrow {}^4I_{9/2}$, $^4F_{3/2} \rightarrow {}^4I_{11/2}$, and $^4F_{3/2} \rightarrow {}^4I_{13/2}$ recorded at RT and 77K. The difference observed from RT to 77 K is a sharpening of the bands and changes in the relative intensities. No changes in the position of the lines i.e. the energies of the electronic states were observed. We assign the broadening to arise from a combination of the inherent properties of the electronic transitions and inhomogeneous broadening related to small variations in site symmetry induced by thermal fluctuations. We assign the change in relative intensities to arise from differences in the relative thermal population of the two emitting states in the $^4F_{3/2}$ multiplet. This can be used in the deconvolution of the electronic structure.[27] The method relies on using the Boltzmann population to deconvolute each band into individual lines. Briefly, the $^4F_{3/2} \rightarrow {}^4I_{9/2}$ band has 10 possible lines. Cursory inspection of the $^4F_{3/2} \rightarrow {}^4I_{9/2}$ band in Figure 3 reveals 4 peaks, at 77K each has a shoulder on the high-energy side. The

shoulder is higher in relative intensity at RT than at 77 K in all peaks, i.e. the lines corresponding to the shoulders are all thermally populated and must be from $^4F_{3/2}(1) \rightarrow {}^4I_J$ transitions. Similarly, the same trends are found in $^4F_{3/2} \rightarrow {}^4I_{11/2}$ and $^4F_{3/2} \rightarrow {}^4I_{13/2}$. These observations can be rationalized by a combined model where $^4F_{3/2}$ is split by ~40 cm^{-1}, which then can be used to deduce the splitting of all five Kramers doublets $^4I_{9/2}$. The model is evaluated for both the emission and excitation spectra in Figure S6. Following this model, all lines in the three emission bands are fitted with a sum of Voigt functions and these are shown in Figure 3 (See Tables S5-S7 for fit details). The fit procedure follows the methodology from previous work.[27] The Gaussian contribution to the broadness of the Voigt function and the energy splitting between $^4F_{3/2}(0)$ and $^4F_{3/2}(1)$ were determined as shared global parameters for each band. The fits are included in Figure 3 and the energies of determined electronic states are compiled in Table 2. We note that the splitting of $^4F_{3/2}$ was found to be 36.5 ± 0.45 cm^{-1}, 40.21 ± 0.08 cm^{-1}, and 39.27 ± 0.08 cm^{-1} in the $^4F_{3/2} \rightarrow {}^4I_{9/2}$, $^4F_{3/2} \rightarrow {}^4I_{11/2}$, and $^4F_{3/2} \rightarrow {}^4I_{13/2}$ bands respectively, the difference is assumed to be the intrinsic experimental error. A weighted average of the three experimentally obtained values obtained from the different bands gives results in 39.5 ± 1.0 cm^{-1} for the splitting of $^4F_{3/2}$.

Table 2. The 20 lowest energy (cm^{-1}) Kramers doublets that could be experimentally resolved. The experimental values are determined from spectroscopy and the calculated values are computed at the RASSCF level. Additionally, the difference between experiment and calculation has been provided in both absolute units and as the deviation in percentage.

State	Exp. (cm^{-1})	calc. (cm^{-1})	Δ (cm^{-1})	Δ (%)
$^4I_{9/2}$ (0)	0	0	-	-
$^4I_{9/2}$ (1)	24.3	29.5	5.2	19
$^4I_{9/2}$ (2)	159.3	152.3	-7.0	4
$^4I_{9/2}$ (3)	298.4	256.8	41.7	15
$^4I_{9/2}$ (4)	434.3	333.1	101.2	26

$^4I_{11/2}$ (0)	1982.1	2192.4	-210.3	10
$^4I_{11/2}$ (1)	2003.5	2214.4	-210.9	10
$^4I_{11/2}$ (2)	2039.7	2253.1	-213.4	10
$^4I_{11/2}$ (3)	2120.1	2311.7	-191.6	9
$^4I_{11/2}$ (4)	2165.8	2331.8	-166.0	7
$^4I_{11/2}$ (5)	2210.8	2346.1	-135.3	6
$^4I_{13/2}$ (0)	3922.5	4417.9	-495.5	12
$^4I_{13/2}$ (1)	3961.9	4457.2	-495.2	12
$^4I_{13/2}$ (2)	3984.0	4475.9	-491.9	12
$^4I_{13/2}$ (3)	4092.0	4562.8	-470.8	11
$^4I_{13/2}$ (4)	4121.2	4577.3	-456.1	10
$^4I_{13/2}$ (5)	4163.3	4596.2	-432.9	10
$^4I_{13/2}$ (6)	4238.2	4639.5	-401.3	9
$^4F_{3/2}$ (0)	11491.1	16193.7	-4702.6	34
$^4F_{3/2}$ (1)	11452.1	16251.1	-4799.0	35

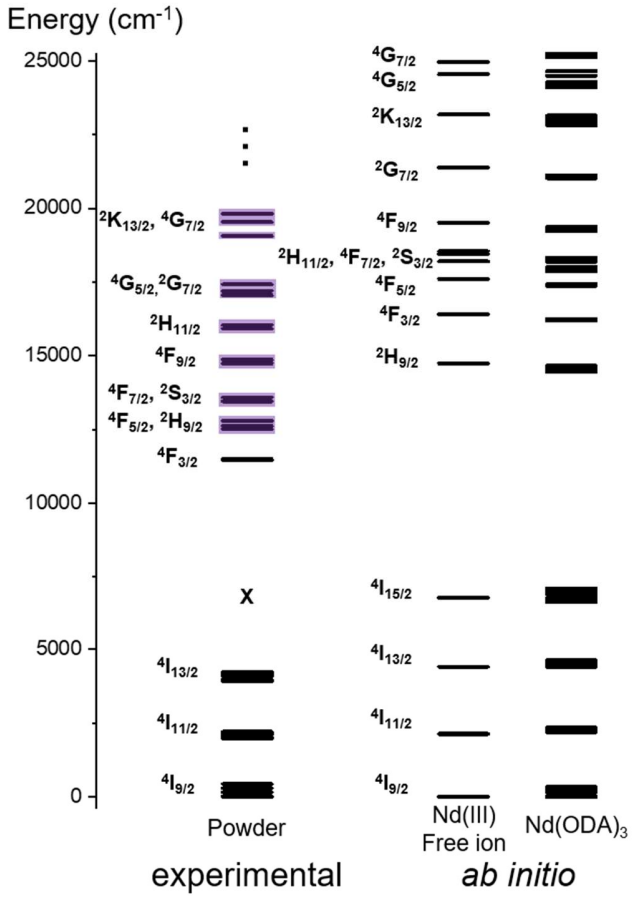

Figure 4. Experimentally determined energy state and *ab initio* calculated energy states at the SA-RAS[3,0,2,0,7,5]SCF/RASSI-SO level. Excited states above the emitting state $^4F_{3/2}$ are not individually resolved experimentally. Instead, the position of the multiplets is shown and a purple transparent box visualizes the broadness of the observed bands in which the individual Kramers doublets are found. Results from calculations are provided for both the free ion and the $Nd(ODA)_3$ complex.

The excitation spectra are likewise used to extract the energy of states above $^4F_{3/2}$ (See Figures S7-S10 and Tables S8-14). However, here we are limited by an experimental resolution of 1-2 nm and the energy of each Kramers doublet cannot be reported. Figure 4 shows the collection of all experimentally determined energy levels of neodymium(III) in the D_3 symmetric $Nd(ODA)_3$ system. The emission spectra have a spectral resolution of 0.4 nm, which makes it possible to extract the energies of the individual Kramers doublets. The 1-2 nm resolution of the excitation spectra limits us to report only multiplet energies, these are plotted with a purple background that illustrates the broadness of the multiplets in which the energies of the individual states can lie.

Calculated electronic structure

Calculations of the electronic structure of neodymium(III) have been carried out following multiple procedures both at the CASSCF and the RASSCF level as discussed in the supporting information (See Tables S15-17). In short, we found the choice of basis set and geometry considerations to be of little significance to the calculated properties. However, the inclusion of the 5*d* electrons in the RAS3 space was needed to reproduce two isolated energy states for the emitting state $^4F_{3/2}$. Resultantly, all computational results discussed in the following are performed at the SA-RAS[3,0,2,0,7,5]SCF/RASSI-SO level (see computational details) on $Nd(ODA)_3$ geometry shown in Figure 1 with hydrogen atomic positions optimized with DFT. The 7 average

natural orbitals used in the RAS2 space that are of pure 4*f* character of neodymium(III) ion and the 5 average natural orbitals used in the RAS3 space that are primarily of 5*d* character of neodymium(III) ion are shown in Figures S13-14. The composition of the wave functions of the $^4I_{9/2}$ term is provided in Table S19.

Figure 4 compares the computed energy levels for both the free neodymium(III) ion and the $Nd(ODA)_3$ complex with the experimentally determined energy levels. An immediate glance reveals that the ^4I_J levels are accurately positioned in energies, while higher energy levels deviate from experimental values. This deviation is increasingly larger as the energy is increased. The lowest energy states in the $^4I_{11/2}$, $^4I_{13/2}$, and $^4F_{3/2}$ multiplets are computed to be 210, 496, and 4703 cm^{-1} higher in energy than the experimentally determined values (see Table 2). Despite the larger deviations as the energy increases, the relative order of quartets and the relative order of doublets follow the expected relative energy patterns within the same spin multiplicity as is expected from Carnall.[99] However, this is not the case for relative energies between the two spin multiplicities. In particular, the $^2H_{9/2}$ multiplet has a lower energy than the $^4F_{3/2}$ multiplet and, despite many attempts, does not provide an accurate relative energy of the emitting multiplet at this level of calculation. To quantify the energy of individual Kramers doublets within $^4I_{9/2}$, $^4I_{11/2}$, and $^4I_{13/2}$ multiplets are, with an average difference of ~10 % in agreement with the experiment (Table 2), while the average difference for the $^4F_{3/2}$ multiplet is calculated to be 35 %. We conclude that the energy levels within ^4I_J are well reproduced by calculations, while the levels at higher energies require new developments of in theory and methodology.

Next, we delve into the splitting within each multiplet, i.e. the crystal field splitting. Figure 5 shows the extracted electronic states in $^4I_{9/2}$, $^4I_{11/2}$, and $^4I_{13/2}$ multiplets superimposed on the emission spectra, and $^4F_{3/2}$ superimposed on the excitation spectra, respectively, compared with

the *ab initio* results. In the figure, the energy of $^4I_{11/2}$, $^4I_{13/2}$, and $^4F_{3/2}$ multiplets are manually decreased by 210 cm^{-1}, 496 cm^{-1}, and 4703 cm^{-1} such that the lowest energy Kramers doublet in each multiplet is the same for calculation and experiment. After this adjustment, the calculations are found to represent the crystal field splitting very well; the qualitative ordering and energy spacing within each multiplet accurately follow the experimental results. The absolute splitting, i.e. the energy difference between the highest and lowest Kramers doublets, in the ^4I_J multiplets are calculated to be 333 cm^{-1}, 154 cm^{-1}, and 222 cm^{-1}, slightly smaller than anticipated from the experiment, where they are found to be 434 cm^{-1}, 229 cm^{-1}, and 316 cm^{-1} respectively. However, an error of this relative magnitude is commonly observed for calculations at this level of theory and similar discrepancies in absolute crystal field splitting have been reported elsewhere.[29] It is concluded that the qualitatively observed splitting is well reproduced, although the calculated total splitting of the multiplets is lower in the calculation. We thus report here that the *ab initio* crystal field calculation of the 18 lowest Kramers doublets and the two emitting Kramers doublets of neodymium(III) in the $Nd(ODA)_3$ complex is in good agreement with experiments.

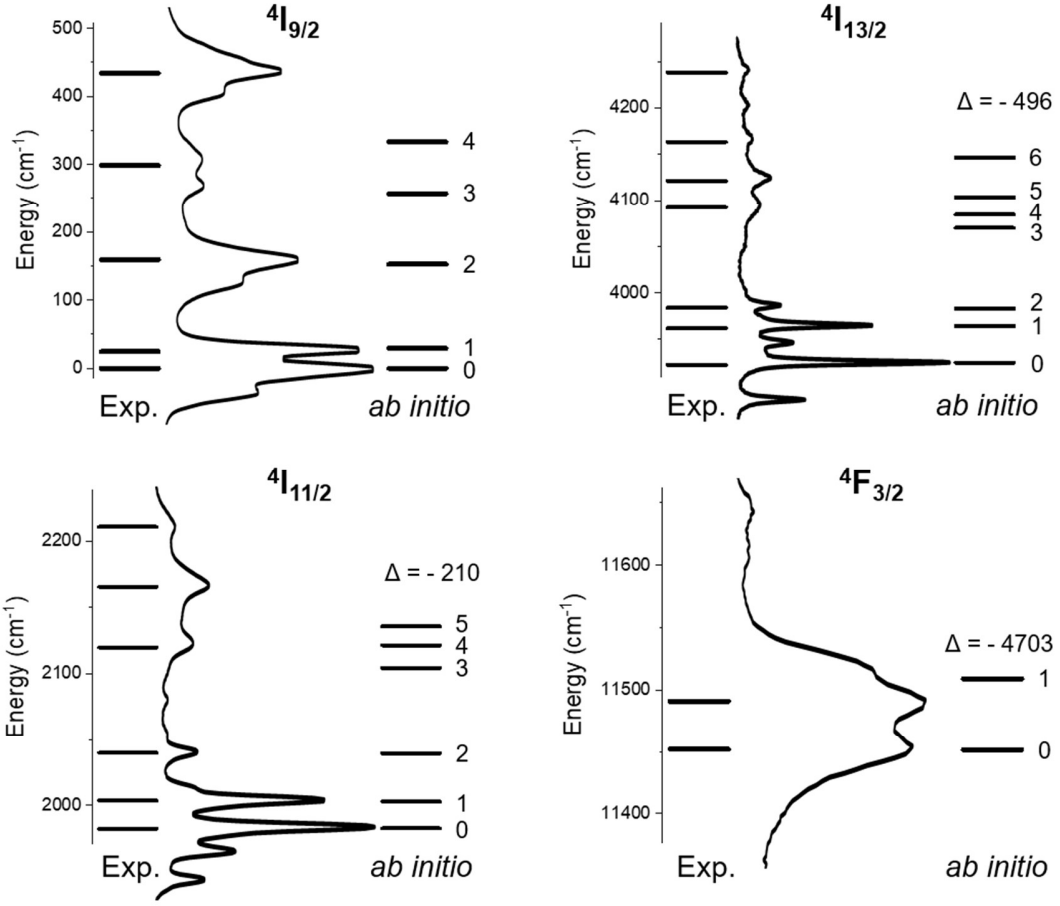

Figure 5. Comparison of the experimentally obtained energy levels of $^4I_{9/2}$ (top left), $^4I_{11/2}$ (bottom left), $^4I_{13/2}$ (top right), and $^4F_{3/2}$ (bottom right) with the SA-RAS[3,0,2,0,7,5]SCF/RASSI-SO calculated energy levels. For visual purposes, the emission spectra collected at 77 K corresponding to each transition are provided. The energy of each calculated Kramers doublet is manually decreased such that the energy of the lowest Kramers doublet is the same as in the experiment. There are reduced by 0, 210, 493, and 4740 cm^{-1} for $^4I_{9/2}$, $^4I_{11/2}$, $^4I_{13/2}$ and $^4F_{3/2}$ respectively.

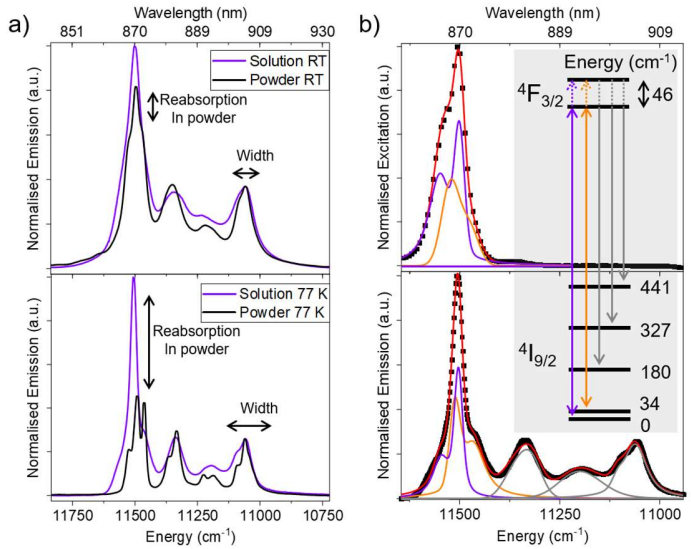

Figure 6. Emission spectra of 20mM Nd(III) in a 60 mM H_2ODA/D_2O solution. a) Compared to the emission spectra of $Na_3[Nd(ODA)_3]\cdot 10H_2O$ crystals dispersed in 2-methyltetrahydrofuran measured at RT (top) and 77 K (bottom). The spectra are normalized to the lowest energy transition, as this does not display any reabsorption. b) The solution spectra at 77 K, excitation (top) and emission (bottom) have been fitted with a sum of Voigt functions. The inlet shows the fit model.

A comment on solution structure

Now that the electronic structure of neodymium(III) in the $Nd(ODA)_3$ has been examined experimentally and compared with *ab initio* evaluation we dare expand on these results to comment on the possible solution structure of this complex. Figure 6a shows the luminescence spectra of $Nd(ODA)_3$ in deuterated water and the dispersed crystalline powder at both RT and 77 K (see Figure S15 for the excitation spectra). Two significant differences are observed between the dispersed powder and the solution, i.e. the relative intensity of the first band is significantly greater in solution, and the bands are broader in solution. Looking at the data in Figure 6a, it should

be noted that a significant degree of reabsorption (cf. inner filter effect) was observed in the low energy band for the powder samples (see Figure S11). The solution spectra are measured at 20 mM and do not have an absorbance above 0.1, and thus no significant inner filter effects. The broadening observed in solution can be attributed to a greater degree of structural fluctuation than in the solid state.

To quantify, the spectra were fitted and compared. A fitting procedure similar to what is done for the dispersed powder at 77 K (see Figure 3) is performed. In Figure 6b, the excitation spectra and the emission spectra of the frozen solution have been fitted with five sets of two Voigt functions separated with a global parameter for the energy splitting in $^4F_{3/2}$ multiplet. Contrary to the powder spectra, it was not possible to fully resolve all 10 lines in the emission spectrum due to the slightly broader peaks. However, with the inclusion of the excitation spectrum in the analysis the splitting can be elucidated. At 77 K only two states are populated in $^4I_{9/2}$ and therefore only transitions from these can be seen in the excitation spectra. These states are very close in energy (see Figure 6b). Fully refining the sum of Voigt functions the model shown in Figure 6b is obtained (see Tables S20-21 for fit details). The crystal field splitting in the emitting multiplet $^4F_{3/2}$ and lowest energy multiplet $^4I_{9/2}$ are found to be nearly identical in the solution and the solid state. In fact, if all peak positions are fixed to the model found in Figure 3, the fit still provides reasonable and statistically acceptable results (see Figure S16 and Tables S22-24). On average the Gaussian and Lorentzian width increase from 16 to 49 cm^{-1} and from 57 to 58 cm^{-1} at 300 K respectively. At 77 K the increase is 11 to 24 cm^{-1} and 27 to 58 cm^{-1}. We thus conclude that the solution structure of $Nd(ODA)_3$ in water is very similar—if not identical—to the powder structure and that the difference in peak broadness can be explained by structural fluctuation alone.

Empirical trends in crystal field splitting

With the electronic structure of the D_3 symmetric $Nd(ODA)_3$ complex mapped, we provide one of the puzzle pieces needed to build strong structure-property relationships for the trivalent neodymium ion. Figure 7 shows the electronic structure of the lowest energy multiplet, $^4I_{9/2}$, of 10 neodymium(III) complexes found in the literature[27, 100-112] including the results reported in this work. The point group symmetry analysis, as detailed above, is applied to all 10 complexes and the structures have been grouped based on their determined point group symmetry (See Tables S25-26).

The literature on the electronic structure of neodymium(III) is not as rich in information as it is for e.g. europium(III), where strong empirical correlations are found between the electronic structure and the point group of the coordination complex.[24, 113] Yet, by cursory inspection of the energy diagram in Figure 7, it appears that trends between the crystal field splitting in $^4I_{9/2}$ and the point group symmetries of the complexes can be observed. The four complexes of D_{3h} symmetry share the same qualitative splitting with the five Kramers doublets grouped in a (1, 2, 2) structure. By removing the horizontal mirror plane in the D_{3h} group, the symmetry can be reduced to D_3, C_{3v}, and C_3. It is found that none of the four complexes with these point groups can be classified with a (1, 2, 2) grouping. Furthermore, it is found that the two structures with D_3 symmetry, one of which is the $Nd(ODA)_3$ reported here, share a splitting that appears to group into a (2, 1, 1, 1) grouping. Moving away from the C_3 symmetric structures altogether, S_4 and D_4, are found to bear little resemblance to the other structures, but share a similar overall crystal field splitting. The 10 structures presented here are not sufficient to construct strict empirical symmetry rules relating property, electronic structure, and site symmetry, but it is an empirical starting point in the structure-property relationships for the trivalent neodymium(III) ion.

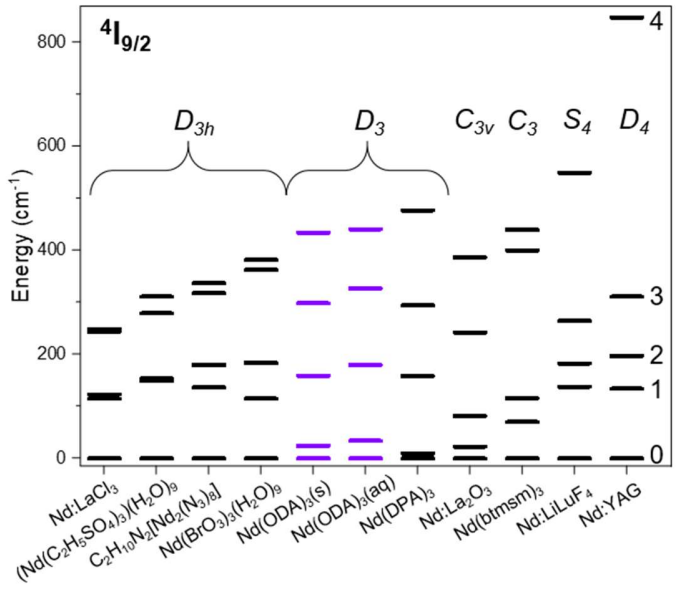

Figure 7. The splitting of the lowest energy multiplet $^4I_{9/2}$ of 9 neodymium(III) complexes from the literature (black) and the Nd(ODA)$_3$ complex reported in this work (purple). The complexes are grouped by point group symmetry. The Kramers doublets are reported for: Nd:LaCl$_3$,[100] (Nd(C$_2$H$_5$SO$_4$)$_3$)(H$_2$O)$_9$,[101] C$_2$H$_{10}$N$_2$[Nd$_2$(N$_3$)$_8$],[102] Nd(BrO$_3$)$_3$(H$_2$O)$_9$,[103] solid state Nd(ODA)$_3$ (this work), aqueous Nd(ODA)$_3$ (this work), Nd(DPA)$_3$,[27] Nd:La$_2$O$_3$,[104] Nd(btmsm)$_3$,[105] Nd:LiLuF$_4$,[106] and Nd:YAG.[107]

Conclusion

The crystal structure, symmetry, luminescent properties, and electronic structure of a neodymium(III) tris(oxydiacetate) complex were reported, and the results were used to evaluate the extent to which *ab initio* calculations provide an electronic structure comparable to that measured. High-resolution optical spectroscopy, near-infrared excitation and emission spectra were used to determine all electronic transitions of neodymium(III) in the range 500 nm to 1400 nm. A Boltzmann analysis and a spectral deconvolution of all 20 Kramers doublets in the emitting $^4F_{3/2}$ multiplet, and the three low energy $^4I_{9/2}$, $^4I_{11/2}$, and $^4I_{13/2}$ multiplets were experimentally determined. In particular, the crystal field splitting of the $^4I_{9/2}$ multiplet is reported as 0, 24, 159, 298, and 434, or a (2, 1, 1, 1) grouping of Kramers doublets for the D_3 symmetric complex.

The assignment of energy levels was critically evaluated with *ab initio* calculations at the RASSCF level to investigate the accuracy of which the experimental energy levels were reproduced. Despite difficulties in the calculation of energy levels with higher energies than the emissive $^4F_{3/2}$ multiplet, we report accurate reproduced relative energies for all Kramers doublets within the $^4I_{9/2}$, $^4I_{11/2}$, $^4I_{13/2}$, and $^4F_{3/2}$ multiplets with a ~10 % absolute difference from the experimentally determined values in ^4I_J. In particular, we found the crystal field splitting, which is directly tied to the chemical structure, to be well described. We conclude that the *ab initio* calculations at the RASSCF level fully reproduce the electronic structure in the ^4I_J multiplets.

Furthermore, we examine the subtle changes in the emission spectra of the $Nd(ODA)_3$ complex in the solution phase. Our findings indicate that the electronic structure extracted experimentally is a near-perfect match to the solid state suggesting that the complex maintains its structural integrity when dissolved in water.

The work presented here provides what is—to our knowledge—the most comprehensive evaluation of the electronic structure of neodymium(III) resolved from luminescence spectroscopy. We also collected the well-resolved crystal field splitting of nine neodymium(III) complexes from the literature as a first step towards elucidating the structure-property relationships governing the neodymium(III) ion.

ASSOCIATED CONTENT

Supporting Information. Additional experimental data, fitting of high resolution emission spectra, crystallographic data, symmetry determination and computational details are available as Supporting Information

The following files are available free of charge.

Supporting information (.PDF)

AUTHOR INFORMATION

Corresponding Author

* TJS@chem.ku.dk

Funding Sources

The Carlsberg Foundation, Villum Fonden, Novo Nordisk Fonden, Independent Research Fund Denmark, Tranes Foundation, and the William Demand Foundation.

ACKNOWLEDGMENT

We thank the Carlsberg Foundation, Villum Fonden, Novo Nordisk Fonden, Independent Research Fund Denmark, Tranes Foundation, the William Demand Foundation, and the University of Copenhagen for generous support.

REFERENCES

(1) Haynam, C. A.; Wegner, P. J.; Auerbach, J. M.; Bowers, M. W.; Dixit, S. N.; Erbert, G. V.; Heestand, G. M.; Henesian, M. A.; Hermann, M. R.; Jancaitis, K. S.; et al. National Ignition Facility Laser Performance Status. *Appl. Opt.* **2007**, *46* (16), 3276-3303.
(2) Campbell, J. H.; Suratwala, T. I. Nd-Doped Phosphate Glasses for High-Energy/High-Peak-Power Lasers. *Journal of Non-Crystalline Solids* **2000**, *263-264*, 318-341.
(3) Lu, J.; Ueda, K.-i.; Yagi, H.; Yanagitani, T.; Akiyama, Y.; Kaminskii, A. A. Neodymium Doped Yttrium Aluminum Garnet (Y3al5o12) Nanocrystalline Ceramics—a New Generation of Solid State Laser and Optical Materials. *Journal of Alloys and Compounds* **2002**, *341* (1), 220-225.
(4) Sagawa, M.; Fujimura, S.; Togawa, N.; Yamamoto, H.; Matsuura, Y. New Material for Permanent Magnets on a Base of Nd and Fe (Invited). *Journal of Applied Physics* **1984**, *55* (6), 2083-2087.
(5) Sugimoto, S. Current Status and Recent Topics of Rare-Earth Permanent Magnets. *Journal of Physics D: Applied Physics* **2011**, *44* (6), 064001.
(6) Rinehart, J. D.; Long, J. R. Exploiting Single-Ion Anisotropy in the Design of F-Element Single-Molecule Magnets. *Chemical Science* **2011**, *2* (11), 2078-2085.

(7) Bünzli, J.-C. G. Lanthanide Luminescence for Biomedical Analyses and Imaging. *Chemical Reviews* **2010**, *110* (5), 2729-2755.
(8) Berezin, M. Y.; Achilefu, S. Fluorescence Lifetime Measurements and Biological Imaging. *Chemical Reviews* **2010**, *110* (5), 2641-2684.
(9) Wang, X.; Chang, H.; Xie, J.; Zhao, B.; Liu, B.; Xu, S.; Pei, W.; Ren, N.; Huang, L.; Huang, W. Recent Developments in Lanthanide-Based Luminescent Probes. *Coordination Chemistry Reviews* **2014**, *273-274*, 201-212.
(10) Matulionyte, M.; Skripka, A.; Ramos-Guerra, A.; Benayas, A.; Vetrone, F. The Coming of Age of Neodymium: Redefining Its Role in Rare Earth Doped Nanoparticles. *Chemical Reviews* **2023**, *123* (1), 515-554.
(11) Xie, X.; Gao, N.; Deng, R.; Sun, Q.; Xu, Q.-H.; Liu, X. Mechanistic Investigation of Photon Upconversion in Nd3+-Sensitized Core–Shell Nanoparticles. *Journal of the American Chemical Society* **2013**, *135* (34), 12608-12611.
(12) Back, M.; Ueda, J.; Xu, J.; Murata, D.; Brik, M. G.; Tanabe, S. Ratiometric Luminescent Thermometers with a Customized Phase-Transition-Driven Fingerprint in Perovskite Oxides. *ACS Applied Materials & Interfaces* **2019**, *11* (42), 38937-38945.
(13) Rocha, J.; Brites, C. D. S.; Carlos, L. D. Lanthanide Organic Framework Luminescent Thermometers. *Chemistry – A European Journal* **2016**, *22* (42), 14782-14795.
(14) Cadiau, A.; Brites, C. D. S.; Costa, P. M. F. J.; Ferreira, R. A. S.; Rocha, J.; Carlos, L. D. Ratiometric Nanothermometer Based on an Emissive Ln3+-Organic Framework. *ACS Nano* **2013**, *7* (8), 7213-7218.
(15) Suta, M.; Antić, Ž.; Đorđević, V.; Kuzman, S.; Dramićanin, M. D.; Meijerink, A. Making Nd3+ a Sensitive Luminescent Thermometer for Physiological Temperatures—an Account of Pitfalls in Boltzmann Thermometry. In *Nanomaterials*, 2020; Vol. 10.
(16) Zhao, M.; Li, B.; Wu, Y.; He, H.; Zhu, X.; Zhang, H.; Dou, C.; Feng, L.; Fan, Y.; Zhang, F. A Tumor-Microenvironment-Responsive Lanthanide–Cyanine Fret Sensor for Nir-Ii Luminescence-Lifetime in Situ Imaging of Hepatocellular Carcinoma. *Advanced Materials* **2020**, *32* (28), 2001172.
(17) Bonnet, C. S.; Buron, F.; Caillé, F.; Shade, C. M.; Drahoš, B.; Pellegatti, L.; Zhang, J.; Villette, S.; Helm, L.; Pichon, C.; et al. Pyridine-Based Lanthanide Complexes Combining Mri and Nir Luminescence Activities. *Chemistry – A European Journal* **2012**, *18* (5), 1419-1431.
(18) Song, X.; Li, S.; Guo, H.; You, W.; Shang, X.; Li, R.; Tu, D.; Zheng, W.; Chen, Z.; Yang, H.; et al. Graphene-Oxide-Modified Lanthanide Nanoprobes for Tumor-Targeted Visible/Nir-Ii Luminescence Imaging. *Angewandte Chemie International Edition* **2019**, *58* (52), 18981-18986.
(19) Uh, H.; Petoud, S. Novel Antennae for the Sensitization of near Infrared Luminescent Lanthanide Cations. *Comptes Rendus Chimie* **2010**, *13* (6), 668-680.
(20) Lazarides, T.; Davies, G. M.; Adams, H.; Sabatini, C.; Barigelletti, F.; Barbieri, A.; Pope, S. J. A.; Faulkner, S.; Ward, M. D. Ligand-Field Excited States of Hexacyanochromate and Hexacyanocobaltate as Sensitisers for near-Infrared Luminescence from Nd(Iii) and Yb(Iii) in Cyanide-Bridged D–F Assemblies. *Photochemical & Photobiological Sciences* **2007**, *6* (11), 1152-1157.
(21) Torelli, S.; Imbert, D.; Cantuel, M.; Bernardinelli, G.; Delahaye, S.; Hauser, A.; Bünzli, J.-C. G.; Piguet, C. Tuning the Decay Time of Lanthanide-Based near Infrared Luminescence from Micro- to Milliseconds through D→F Energy Transfer in Discrete Heterobimetallic Complexes. *Chemistry – A European Journal* **2005**, *11* (11), 3228-3242.

(22) Hilderbrand, S. A.; Weissleder, R. Near-Infrared Fluorescence: Application to in Vivo Molecular Imaging. *Curr Opin Chem Biol* **2010**, *14* (1), 71-79.
(23) Nawrocki, P.; Sørensen, T. J. Optical Spectroscopy as a Tool for Studying the Solution Chemistry of Neodymium(Iii). *Physical Chemistry Chemical Physics* **2023**.
(24) Binnemans, K. Interpretation of Europium(Iii) Spectra. *Coordination Chemistry Reviews* **2015**, *295*, 1-45.
(25) Faulkner, S.; Carrié, M.-C.; Pope, S. J. A.; Squire, J.; Beeby, A.; Sammes, P. G. Pyrene-Sensitised near-Ir Luminescence from Ytterbium and Neodymium Complexes. *Dalton Transactions* **2004**, (9), 1405-1409, 10.1039/B401302F.
(26) Beeby, A.; Faulkner, S. Luminescence from Neodymium(Iii) in Solution. *Chemical Physics Letters* **1997**, *266* (1), 116-122.
(27) Nielsen, V. R. M.; Nawrocki, P. R.; Sørensen, T. J. Electronic Structure of Neodymium(Iii) and Europium(Iii) Resolved in Solution Using High-Resolution Optical Spectroscopy and Population Analysis. *The Journal of Physical Chemistry A* **2023**.
(28) Kofod, N.; Nawrocki, P.; Platas-Iglesias, C.; Sørensen, T. J. Electronic Structure of Ytterbium(Iii) Solvates - a Combined Spectroscopic and Theoretical Study. *Inorganic Chemistry* **2021**, *60* (10), 7453-7464.
(29) Ungur, L.; Chibotaru, L. F. Ab Initio Crystal Field for Lanthanides. *Chemistry - A European Journal* **2017**, *23* (15), 3708-3718.
(30) Alessandri, R.; Zulfikri, H.; Autschbach, J.; Bolvin, H. Crystal Field in Rare-Earth Complexes: From Electrostatics to Bonding. *Chemistry – A European Journal* **2018**, *24* (21), 5538-5550.
(31) Bi, Y.; Chen, C.; Zhao, Y.-F.; Zhang, Y.-Q.; Jiang, S.-D.; Wang, B.-W.; Han, J.-B.; Sun, J.-L.; Bian, Z.-Q.; Wang, Z.-M.; et al. Thermostability and Photoluminescence of Dy(Iii) Single-Molecule Magnets under a Magnetic Field. *Chemical Science* **2016**, *7* (8), 5020-5031, 10.1039/C6SC01157H.
(32) Norel, L.; Darago, L. E.; Le Guennic, B.; Chakarawet, K.; Gonzalez, M. I.; Olshansky, J. H.; Rigaut, S.; Long, J. R. A Terminal Fluoride Ligand Generates Axial Magnetic Anisotropy in Dysprosium Complexes. *Angewandte Chemie International Edition* **2018**, *57* (7), 1933-1938.
(33) Gendron, F.; Di Pietro, S.; Abad Galán, L.; Riobé, F.; Placide, V.; Guy, L.; Zinna, F.; Di Bari, L.; Bensalah-Ledoux, A.; Guyot, Y.; et al. Luminescence, Chiroptical, Magnetic and Ab Initio Crystal-Field Characterizations of an Enantiopure Helicoidal Yb(Iii) Complex. *Inorganic Chemistry Frontiers* **2021**, *8* (4), 914-926.
(34) Pointillart, F.; le Guennic, B.; Cador, O.; Maury, O.; Ouahab, L. Lanthanide Ion and Tetrathiafulvalene-Based Ligand as a "Magic" Couple toward Luminescence, Single Molecule Magnets, and Magnetostructural Correlations. *Accounts of Chemical Research* **2015**, *48* (11), 2834-2842.
(35) Cosquer, G.; Pointillart, F.; Jung, J.; Le Guennic, B.; Golhen, S.; Cador, O.; Guyot, Y.; Brenier, A.; Maury, O.; Ouahab, L. Alkylation Effects in Lanthanide Complexes Involving Tetrathiafulvalene Chromophores: Experimental and Theoretical Correlation between Magnetism and near-Infrared Emission. *European Journal of Inorganic Chemistry* **2014**, *2014* (1), 69-82.
(36) Long, J.; Guari, Y.; Ferreira, R. A. S.; Carlos, L. D.; Larionova, J. Recent Advances in Luminescent Lanthanide Based Single-Molecule Magnets. *Coordination Chemistry Reviews* **2018**, *363*, 57-70.
(37) Pointillart, F.; Cador, O.; Le Guennic, B.; Ouahab, L. Uncommon Lanthanide Ions in Purely 4f Single Molecule Magnets. *Coordination Chemistry Reviews* **2017**, *346*, 150-175.

(38) Cucinotta, G.; Perfetti, M.; Luzon, J.; Etienne, M.; Car, P.-E.; Caneschi, A.; Calvez, G.; Bernot, K.; Sessoli, R. Magnetic Anisotropy in a Dysprosium/Dota Single-Molecule Magnet: Beyond Simple Magneto-Structural Correlations. *Angewandte Chemie International Edition* **2012**, *51* (7), 1606-1610.
(39) Soussi, K.; Jung, J.; Pointillart, F.; Le Guennic, B.; Lefeuvre, B.; Golhen, S.; Cador, O.; Guyot, Y.; Maury, O.; Ouahab, L. Magnetic and Photo-Physical Investigations into Dyiii and Ybiii Complexes Involving Tetrathiafulvalene Ligand. *Inorganic Chemistry Frontiers* **2015**, *2* (12), 1105-1117, 10.1039/C5QI00087D.
(40) Guettas, D.; Gendron, F.; Fernandez Garcia, G.; Riobé, F.; Roisnel, T.; Maury, O.; Pilet, G.; Cador, O.; Le Guennic, B. Luminescence-Driven Electronic Structure Determination in a Textbook Dimeric Dyiii-Based Single-Molecule Magnet. *Chemistry – A European Journal* **2020**, *26* (19), 4389-4395, https://doi.org/10.1002/chem.201905493.
(41) Raju, M. S.; Dhbaibi, K.; Grasser, M.; Dorcet, V.; Breslavetz, I.; Paillot, K.; Vanthuyne, N.; Cador, O.; Rikken, G. L. J. A.; Le Guennic, B.; et al. Magneto-Chiral Dichroism in a One-Dimensional Assembly of Helical Dysprosium(Iii) Single-Molecule Magnets. *Inorganic Chemistry* **2023**, *62* (43), 17583-17587.
(42) Pederson, R.; Wysocki, A. L.; Mayhall, N.; Park, K. Multireference Ab Initio Studies of Magnetic Properties of Terbium-Based Single-Molecule Magnets. *The Journal of Physical Chemistry A* **2019**, *123* (32), 6996-7006.
(43) Wysocki, A. L.; Park, K. Nature of Hyperfine Interactions in Tbpc2 Single-Molecule Magnets: Multiconfigurational Ab Initio Study. *Inorganic Chemistry* **2020**, *59* (5), 2771-2780.
(44) Brunet, G.; Marin, R.; Monk, M.-J.; Resch-Genger, U.; Gálico, D. A.; Sigoli, F. A.; Suturina, E. A.; Hemmer, E.; Murugesu, M. Exploring the Dual Functionality of an Ytterbium Complex for Luminescence Thermometry and Slow Magnetic Relaxation. *Chemical Science* **2019**, *10* (28), 6799-6808, 10.1039/C9SC00343F.
(45) Pointillart, F.; Guennic, B. L.; Golhen, S.; Cador, O.; Maury, O.; Ouahab, L. A Redox-Active Luminescent Ytterbium Based Single Molecule Magnet. *Chemical Communications* **2013**, *49* (6), 615-617, 10.1039/C2CC37635K.
(46) Dhbaibi, K.; Grasser, M.; Douib, H.; Dorcet, V.; Cador, O.; Vanthuyne, N.; Riobé, F.; Maury, O.; Guy, S.; Bensalah-Ledoux, A.; et al. Multifunctional Helicene-Based Ytterbium Coordination Polymer Displaying Circularly Polarized Luminescence, Slow Magnetic Relaxation and Room Temperature Magneto-Chiral Dichroism**. *Angewandte Chemie International Edition* **2023**, *62* (5), e202215558.
(47) Atzori, M.; Dhbaibi, K.; Douib, H.; Grasser, M.; Dorcet, V.; Breslavetz, I.; Paillot, K.; Cador, O.; Rikken, G. L. J. A.; Le Guennic, B.; et al. Helicene-Based Ligands Enable Strong Magneto-Chiral Dichroism in a Chiral Ytterbium Complex. *Journal of the American Chemical Society* **2021**, *143* (7), 2671-2675.
(48) Jassal, A. K.; Aliaga-Alcalde, N.; Corbella, M.; Aravena, D.; Ruiz, E.; Hundal, G. Neodymium 1d Systems: Targeting New Sources for Field-Induced Slow Magnetization Relaxation. *Dalton Transactions* **2015**, *44* (36), 15774-15778, 10.1039/C5DT02533H.
(49) Chen, Y.-C.; Huang, X.-S.; Liu, J.-L.; Tong, M.-L. Magnetic Dynamics of a Neodymium(Iii) Single-Ion Magnet. *Inorganic Chemistry* **2018**, *57* (18), 11782-11787.
(50) Li, Q.-W.; Wan, R.-C.; Chen, Y.-C.; Liu, J.-L.; Wang, L.-F.; Jia, J.-H.; Chilton, N. F.; Tong, M.-L. Unprecedented Hexagonal Bipyramidal Single-Ion Magnets Based on Metallacrowns. *Chemical Communications* **2016**, *52* (91), 13365-13368, 10.1039/C6CC06924J.

(51) Bartolomé, E.; Arauzo, A.; Luzón, J.; Melnic, S.; Shova, S.; Prodius, D.; Nlebedim, I. C.; Bartolomé, F.; Bartolomé, J. High Relaxation Barrier in Neodymium Furoate-Based Field-Induced Smms. *Dalton Transactions* **2019**, *48* (41), 15386-15396, 10.1039/C9DT02047K.
(52) Gupta, S. K.; Rajeshkumar, T.; Rajaraman, G.; Murugavel, R. An Unprecedented Zero Field Neodymium(Iii) Single-Ion Magnet Based on a Phosphonic Diamide. *Chemical Communications* **2016**, *52* (44), 7168-7171, 10.1039/C6CC03066A.
(53) Kervern, G.; D'Aléo, A.; Toupet, L.; Maury, O.; Emsley, L.; Pintacuda, G. Crystal-Structure Determination of Powdered Paramagnetic Lanthanide Complexes by Proton Nmr Spectroscopy. *Angewandte Chemie International Edition* **2009**, *48* (17), 3082-3086.
(54) Brayshaw, P. A.; Buenzli, J.-C. G.; Froidevaux, P.; Harrowfield, J. M.; Kim, Y.; Sobolev, A. N. Synthetic, Structural, and Spectroscopic Studies on Solids Containing Tris(Dipicolinato) Rare Earth Anions and Transition or Main Group Metal Cations. *Inorganic Chemistry* **1995**, *34* (8), 2068-2076.
(55) Cotton, F. A.; Huang, P. Further Observations on the Non-Rigorous Relationship between Triboluminescence and Crystal Centricity. *Inorganica Chimica Acta* **2003**, *346*, 223-226.
(56) M Albin, R. W., WDW Horrocks Jr Laser Spectroscopic and X-Ray Structural Investigation of Europium (Iii)-Oxydiacetate Complexes in Solution and in the Solid State. *Inorganic Chemistry - ACS Publications* **1985**, *24*, 4591-4594.
(57) Lennartson, A.; Håkansson, M. Total Spontaneous Resolution of Nine-Coordinate Complexes. *CrystEngComm* **2009**, *11* (9), 1979-1986, 10.1039/B903554K.
(58) Albin, M.; Whittle, R. R.; Horrocks, W. D., Jr. Laser Spectroscopic and X-Ray Structural Investigation of Europium(Iii)-Oxydiacetate Complexes in Solution and in the Solid State. *Inorganic Chemistry* **1985**, *24* (26), 4591-4594.
(59) Albertsson, J.; Elding, I. The Hydrogen-Bond System in a Water-Rich Crystalline Hydrate: A Neutron Diffraction Study of Trisodium Tris(Oxydiacetato)Cerate(Iii) Nonahydrate. *Acta Crystallographica Section B* **1976**, *32* (11), 3066-3077.
(60) Qiu, J.-Z.; Wang, L.-F.; Chen, Y.-C.; Zhang, Z.-M.; Li, Q.-W.; Tong, M.-L. Magnetocaloric Properties of Heterometallic 3d–Gd Complexes Based on the [Gd(Oda)3]3− Metalloligand. *Chemistry – A European Journal* **2016**, *22* (2), 802-808.
(61) Kremer, C.; Torres, J.; Domínguez, S. Lanthanide Complexes with Oda, Ida, and Nta: From Discrete Coordination Compounds to Supramolecular Assemblies. *Journal of Molecular Structure* **2008**, *879* (1), 130-149.
(62) Mitcov, D.; Platunov, M.; Buch, C. D.; Reinholdt, A.; Døssing, A. R.; Wilhelm, F.; Rogalev, A.; Piligkos, S. Hard X-Ray Magnetochiral Dichroism in a Paramagnetic Molecular 4f Complex. *Chemical Science* **2020**, *11* (31), 8306-8311, 10.1039/D0SC02709J.
(63) Parac-Vogt, T. N.; Binnemans, K.; Görller-Walrand, C. Absolute Configuration Assignment of D3-Symmetric Lanthanide Complexes Based on Circular Dichroism Induced by Interaction with a Chiral Probe. *ChemPhysChem* **2001**, *2* (12), 767-769.
(64) Sickinger, A.; Baguenard, B.; Bensalah-Ledoux, A.; Guyot, Y.; Guy, L.; Pointillart, F.; Cador, O.; Grasser, M.; Le Guennic, B.; Riobé, F.; et al. Impact of the Experimental Bandwidth on Circularly Polarized Luminescence Measurements of Lanthanide Complexes: The Case of Erbium(Iii). *Journal of Materials Chemistry C* **2024**, *12* (12), 4253-4260, 10.1039/D3TC04717B.
(65) Leonard, J. P.; Jensen, P.; McCabe, T.; O'Brien, J. E.; Peacock, R. D.; Kruger, P. E.; Gunnlaugsson, T. Self-Assembly of Chiral Luminescent Lanthanide Coordination Bundles. *Journal of the American Chemical Society* **2007**, *129* (36), 10986-10987.
(66) Mortensen, S. S.; Nielsen, V. R. M.; Sørensen, T. J. **2024**.

(67) Connolly, B. J. P.; Lian, J. Y. J.; Bernhardt, P. V.; Riley, M. J. Ab Initio Investigation of the Na3[Ln(Oda)3]·2naclo4·6h2o (Ln = Ce–Yb; Oda = Oxydiacetate) Series. *Inorganic Chemistry* **2023**, *62* (4), 1328-1340.
(68) Pointillart, F.; Atzori, M.; Train, C. Magneto-Chiral Dichroism of Chiral Lanthanide Complexes. *Inorganic Chemistry Frontiers* **2024**, *11* (5), 1313-1321, 10.1039/D3QI02510A.
(69) Dolomanov, O. V.; Bourhis, L. J.; Gildea, R. J.; Howard, J. A.; Puschmann, H. Olex2: A Complete Structure Solution, Refinement and Analysis Program. *Journal of applied crystallography* **2009**, *42* (2), 339-341.
(70) Sheldrick, G. M. Crystal Structure Refinement with Shelxl. *Acta Crystallographica Section C: Structural Chemistry* **2015**, *71* (1), 3-8.
(71) Sheldrick, G. M.; Schneider, T. R. [16] Shelxl: High-Resolution Refinement. In *Methods in Enzymology*, Vol. 277; Elsevier, 1997; pp 319-343.
(72) Nawrocki, P. R.; Nielsen, V. M. R.; Sørensen, T. J. A High-Sensitivity Rapid Acquisition Spectrometer for Lanthanide(Iii) Luminescence. *Methods and Applications in Fluorescence* **2022**.
(73) Fdez. Galván, I.; Vacher, M.; Alavi, A.; Angeli, C.; Aquilante, F.; Autschbach, J.; Bao, J. J.; Bokarev, S. I.; Bogdanov, N. A.; Carlson, R. K.; et al. Openmolcas: From Source Code to Insight. *Journal of Chemical Theory and Computation* **2019**, *15* (11), 5925-5964.
(74) Li Manni, G.; Fdez. Galván, I.; Alavi, A.; Aleotti, F.; Aquilante, F.; Autschbach, J.; Avagliano, D.; Baiardi, A.; Bao, J. J.; Battaglia, S.; et al. The Openmolcas Web: A Community-Driven Approach to Advancing Computational Chemistry. *Journal of Chemical Theory and Computation* **2023**, *19* (20), 6933-6991.
(75) Olsen, J.; Roos, B. O.; Jo/rgensen, P.; Jensen, H. J. r. A. Determinant Based Configuration Interaction Algorithms for Complete and Restricted Configuration Interaction Spaces. *The Journal of Chemical Physics* **1988**, *89* (4), 2185-2192.
(76) Roos, B. O. The Complete Active Space Scf Method in a Fock-Matrix-Based Super-Ci Formulation. *International Journal of Quantum Chemistry* **1980**, *18* (S14), 175-189.
(77) Roos, B. O.; Taylor, P. R.; Sigbahn, P. E. M. A Complete Active Space Scf Method (Casscf) Using a Density Matrix Formulated Super-Ci Approach. *Chemical Physics* **1980**, *48* (2), 157-173.
(78) Malmqvist, P. A.; Rendell, A.; Roos, B. O. The Restricted Active Space Self-Consistent-Field Method, Implemented with a Split Graph Unitary Group Approach. *The Journal of Physical Chemistry* **1990**, *94* (14), 5477-5482.
(79) Hess, B. A. Relativistic Electronic-Structure Calculations Employing a Two-Component No-Pair Formalism with External-Field Projection Operators. *Physical Review A* **1986**, *33* (6), 3742-3748.
(80) Hess, B. A. Applicability of the No-Pair Equation with Free-Particle Projection Operators to Atomic and Molecular Structure Calculations. *Physical Review A* **1985**, *32* (2), 756-763.
(81) Douglas, M.; Kroll, N. M. Quantum Electrodynamical Corrections to the Fine Structure of Helium. *Annals of Physics* **1974**, *82* (1), 89-155.
(82) Roos, B. O.; Lindh, R.; Malmqvist, P.-Å.; Veryazov, V.; Widmark, P.-O. Main Group Atoms and Dimers Studied with a New Relativistic Ano Basis Set. *The Journal of Physical Chemistry A* **2004**, *108* (15), 2851-2858.
(83) Widmark, P.-O.; Malmqvist, P.-Å.; Roos, B. O. Density Matrix Averaged Atomic Natural Orbital (Ano) Basis Sets for Correlated Molecular Wave Functions. *Theoretica chimica acta* **1990**, *77* (5), 291-306.

(84) Malmqvist, P. Å.; Roos, B. O.; Schimmelpfennig, B. The Restricted Active Space (Ras) State Interaction Approach with Spin–Orbit Coupling. *Chemical Physics Letters* **2002**, *357* (3), 230-240.
(85) Heß, B. A.; Marian, C. M.; Wahlgren, U.; Gropen, O. A Mean-Field Spin-Orbit Method Applicable to Correlated Wavefunctions. *Chemical Physics Letters* **1996**, *251* (5), 365-371.
(86) Kohn, W.; Sham, L. J. Self-Consistent Equations Including Exchange and Correlation Effects. *Physical Review* **1965**, *140* (4A), A1133-A1138.
(87) Perdew, J. P.; Burke, K.; Ernzerhof, M. Generalized Gradient Approximation Made Simple [Phys. Rev. Lett. 77, 3865 (1996)]. *Physical Review Letters* **1997**, *78* (7), 1396-1396.
(88) te Velde, G.; Bickelhaupt, F. M.; Baerends, E. J.; Fonseca Guerra, C.; van Gisbergen, S. J. A.; Snijders, J. G.; Ziegler, T. Chemistry with Adf. *Journal of Computational Chemistry* **2001**, *22* (9), 931-967.
(89) E. J. Baerends, T. Z., A. J. Atkins, J. Autschbach,O. Baseggio,; D. Bashford, A. B. r., F. M. Bickelhaupt, C. Bo, P. M.Boerrigter,; C. Cappelli, L. C., C. Daul, D. P. Chong, D. V. Chulhai,; L. Deng, R. M. D., J. M. Dieterich, F. Egidi, D. E. Ellis,; M. van Faassen, L. F., T. H. Fischer, A. Fo¨rster, C. Fonseca; Guerra, M. F., A. Ghysels, A. Giammona, S. J. A. van; Gisbergen, A. G., A. W. Go¨tz, J. A. Groeneveld, O. V. Gritsenko,; M. Gru¨ning, S. G., F. E. Harris, P. van den Hoek, Z. Hu,; C. R. Jacob, H. J., L. Jensen, L. Joubert, J. W. Kaminski,; G. van Kessel, C. K. n., F. Kootstra, A. Kovalenko,; et al. Ams 2022.1, Scm, Theoretical Chemistry, Vrije Universiteit, Amsterdam, the Netherlands, 2022. *URL http://www. scm. com 24*.
(90) Lenthe, E. v.; Baerends, E. J.; Snijders, J. G. Relativistic Regular Two-Component Hamiltonians. *The Journal of Chemical Physics* **1993**, *99* (6), 4597-4610.
(91) van Lenthe, E.; Ehlers, A.; Baerends, E.-J. Geometry Optimizations in the Zero Order Regular Approximation for Relativistic Effects. *The Journal of Chemical Physics* **1999**, *110* (18), 8943-8953.
(92) Thomsen, M. S.; Anker, A. S.; Kacenauskaite, L.; Sørensen, T. J. We Are Never Ever Getting (Back to) Ideal Symmetry: Structure and Luminescence in a Ten-Coordinated Europium (Iii) Sulfate Crystal. **2022**.
(93) Nielsen, V. R. M.; Le Guennic, B.; Sørensen, T. J. **2024**.
(94) Albertsson, J. Structural Studies on the Rare Earth Carboxylates. *Acta Chem. Scand* **1970**, *24* (10), 7.
(95) May, P. S.; Jayasankar, C. K.; Richarson, F. S. Crystals Field Energy Levels and Transition Line Strengths of Neodymium in Trigonal Na3[Nd(Oxydiacetate)3]·2naclo4·6h2o. *Chemical Physics* **1989**, *138* (1), 123-138.
(96) Farrugia, L. J.; Peacock, R. D.; Stewart, B. Lanthanide Complexes of 2, 2′-Oxydiacetate: Na5 [M (C4h4o5) 3](Bf4) 2· 6h2o (M= Nd, Sm or Gd). *Acta Crystallographica Section C: Crystal Structure Communications* **2000**, *56* (10), iuc0000241-e0000436.
(97) Albertsson, J. Structural Studies on Rare Earth Carboxylates. 1. Crystal and Molecular Structure of Na3 [M (Ococh2och2oco) 3]. 2naclo4. 6h2o, M= Nd, Gd and Yb. *ACTA CHEMICA SCANDINAVICA* **1968**, *22* (5), 1563-+.
(98) Kirby, A. F.; Richardson, F. Optical Excitation and Emission Spectra of Europium (3+) in Microcrystalline Samples of Trigonal Na3 [Eu (Oda) 3]. 2naclo4. 6h2o. *The Journal of Physical Chemistry* **1983**, *87* (14), 2557-2563.
(99) Carnall, W. T.; Fields, P. R.; Rajnak, K. Electronic Energy Levels in the Trivalent Lanthanide Aquo Ions. I. Pr3+, Nd3+, Pm3+, Sm3+, Dy3+, Ho3+, Er3+, and Tm3+. *The Journal of Chemical Physics* **1968**, *49* (10), 4424-4442.

(100) Carlson, E. H.; Dieke, G. H. The State of the Nd3+ Ion as Derived from the Absorption and Fluorescence Spectra of Ndcl3 and Their Zeeman Effects. *The Journal of Chemical Physics* **1961**, *34* (5), 1602-1609.
(101) Gruber, J. B.; Satten, R. A. Analysis of the Electronic Spectra of Neodymium Ethylsulfate. *The Journal of Chemical Physics* **1963**, *39* (6), 1455-1463.
(102) Starynowicz, P.; Bukietyn´ska, K.; Ryba-Romanowski, W.; Dominiak-Dzik, G.; Goł¸b, S. Spectroscopy and Structure of Complexes with Lnn Bonds (Iii). Structure and Spectroscopy of Ethylenediammonium Octaazi Dodineodymate. *Polyhedron* **1994**, *13* (6), 1069-1075.
(103) Satten, R. A. Analysis of the Spectrum of the Nd+++ Ion in the Bromate Crystal. *The Journal of Chemical Physics* **1953**, *21* (4), 637-648.
(104) Henderson, J. R.; Muramoto, M.; Gruber, J. B. Spectrum of Nd3+ in Lanthanide Oxide Crystals. *The Journal of Chemical Physics* **1967**, *46* (7), 2515-2520.
(105) Guttenberger, C.; Unrecht, B.; Reddmann, H.; Amberger, H. D. Electronic Structures of Organometallic Complexes of F Elements.: Lv. Parametric Analysis of the Crystal Field Splitting Pattern of Tris(Bis(Trimethylsilyl)Methyl)Neodymium(Iii). *Inorganica Chimica Acta* **2003**, *348*, 165-172.
(106) Huang, P.; Zheng, W.; Tu, D.; Shang, X.; Zhang, M.; Li, R.; Xu, J.; Liu, Y.; Chen, X. Unraveling the Electronic Structures of Neodymium in Liluf4 Nanocrystals for Ratiometric Temperature Sensing. *Advanced Science* **2019**, *6* (10), 1802282, https://doi.org/10.1002/advs.201802282.
(107) Koningstein, J. A.; Geusic, J. E. Energy Levels and Crystal-Field Calculations of Neodymium in Yttrium Aluminum Garnet. *Physical Review* **1964**, *136* (3A), A711-A716.
(108) Morosin, B. Crystal Structures of Anhydrous Rare-Earth Chlorides. *The Journal of Chemical Physics* **1968**, *49* (7), 3007-3012.
(109) Thoma, R. E.; Weaver, C. F.; Friedman, H. A.; Insley, H.; Harris, L. A.; Yakel, H. A., Jr. Phase Equilibria in the System Lif—Yf3. *The Journal of Physical Chemistry* **1961**, *65* (7), 1096-1099.
(110) Hitchcock, P. B.; Lappert, M. F.; Smith, R. G.; Bartlett, R. A.; Power, P. P. Synthesis and Structural Characterisation of the First Neutral Homoleptic Lanthanide Metal(Iii) Alkyls: [Lnr3][Ln = La or Sm, R = Ch(Sime3)2]. *Journal of the Chemical Society, Chemical Communications* **1988**, (15), 1007-1009, 10.1039/C39880001007.
(111) Aldebert, P.; Traverse, J. P. Etude Par Diffraction Neutronique Des Structures De Haute Temperature De La2o3 Et Nd2o3. *Materials Research Bulletin* **1979**, *14* (3), 303-323.
(112) Helmholz, L. The Crystal Structure of Neodymium Bromate Enneahydrate, Nd(Bro3)3·9h2o. *Journal of the American Chemical Society* **1939**, *61* (6), 1544-1550.
(113) Tanner, P. A. Some Misconceptions Concerning the Electronic Spectra of Tri-Positive Europium and Cerium. *Chemical Society Reviews* **2013**, *42* (12), 5090-5101, 10.1039/C3CS60033E.